Published in Applied Physics Letters 98, issue 071104, 1-3, 2011
which should be used for any reference to this work

Intersubband spectroscopy probing higher order interminiband transitions in AlN-GaN-based superlattices

Daniel Hofstetter,[1,a)] J. Di Francesco,[1] Prem K. Kandaswamy,[2] and Eva Monroy[2]
[1]*Institute of Physics, University of Neuchatel, Avenue de Bellevaux 51, 2009 Neuchatel, Switzerland*
[2]*CEA Grenoble, INAC/SP2M/NPSC, 17 rue des Martyrs, 38054 Grenoble Cedex 9, France*

We investigate midinfrared intersubband photodetectors based on short-period AlN/GaN superlattices with different quantum well thicknesses. Band structure calculations, as well as optical transmission and photovoltage measurements, underline the importance of higher order interminiband transitions. In particular, it was found that optical transitions between the second and third minibands benefit from much larger electron displacements and oscillator strengths than those between the first and second minibands. Our results suggest that optical rectification is *therefore* much more efficient for devices based on a *higher order interminiband* transition.

Since their demonstration in 2003,[1] intersubband (ISB) photodetectors in III-nitrides have seen a steady progress, which culminated in the demonstration of multigigahertz quantum cascade detectors in 2008.[2] Thanks to the use of quantum dots instead of quantum wells (QWs), a marked performance improvement could recently be achieved.[3] The presence of the wetting layer ground state allows electrons to profit from a longer lifetime and a larger lateral displacement, two features which promote an enhancement of the nonlinear coefficient for optical rectification.[4] Already in 2007, we noticed that sequential two-photon processes involving *higher order* ISB transitions play an important role in III-nitride based photodetectors.[5] Furthermore, the strong electronic coupling in III-nitride superlattices leads to the formation of minibands. Here, we present experimental evidence, which clearly indicates that the dominant ISB transition for optical rectification is the one between the second and the third miniband of the superlattice. In contrast, the main transition for ISB absorption remains the 1 to 2 transition.[6] This is particularly interesting for the photodetector samples: They profit not only from about four times larger oscillator strengths, but also from greatly enhanced lateral electron displacements. In addition, the strongly diagonal nature of the 2 to 3 transition results in a roughly twice as long electron-optical phonon scattering time and a further enhancement of the optical rectification signal. Finally, if the doping density in the ground state is high enough, a non-negligible number of electrons can populate the second miniband, making $2 \rightarrow 3$ transitions ideally suited for photodetection.

The fabrication of these devices was based on plasma-assisted molecular beam epitaxy on AlN-on-sapphire templates.[7] The structure of this series of photodetectors has been varied in only one parameter, namely, the thickness of the QW layers. On top of a 1 μm thick undoped AlN buffer, we grew a 40 period superlattice with 1.7 nm thick undoped AlN barrier layers and nominally 2.8 (sample A), 2.3 (sample B), 1.8 (sample C), and 1.3 nm thick (sample D) doped ($[\mathrm{Si}]=5\times10^{19}$ cm^{-3}) GaN QWs. The superlattice was then covered with an undoped 50 nm AlN cap. Both superlattice period and QW/barrier thicknesses were found in excellent agreement with values obtained via high resolution ω-2θ x-ray diffraction scans around (006) and reciprocal space maps around (10-5) crystalline reflections. For transmission measurements, the samples were equipped with two parallel polished 45° facets to form a roughly 3 mm long multipass waveguide. On the surface, 0.8 mm wide and 3 mm long metal stripes (Ti/Au, 10/300 nm) were thermally evaporated. After being mounted on copper heatsinks, the detectors were wire bonded to Au-coated ceramic bonding pads. As shown in Fig. 1(d) of Ref. 5, photovoltage signals are measured between the dark reference contact and the illuminated signal contact. The signals are amplified using a low noise current amplifier (SR570) and fed into the external detector port of a Bruker IFS-66 Fourier transform infrared spectrometer. The detector performance was measured as a function of temperature by mounting the samples into a liquid He flow cryostat.

For the band structure calculations, which were performed with the Schrödinger equation solver "CALCULEBAND" developed at the University of Neuchâtel, effective masses of $0.22m_e$ for GaN and $0.32m_e$ for AlN, a non-parabolicity of 5×10^{-20} m^2, and a band discontinuity of 1.9 eV were used. The schematic band structure in Fig. 1 (left) shows that strong coupling present in such superlattices forms minibands having an increasing width for larger quantum numbers. As outlined in our earlier publications on III-nitride based photodetectors, the working principle of such devices is optical rectification, where electrons excited into an upper miniband undergo a lateral (in growth direction) displacement. This displacement leads to polarization and a measurable photovoltage.[3,4] Especially for the thin samples C and D, transitions from the second into the third miniband are particularly favorable, because in this case the third miniband extends into the triangular part of the AlN barrier. In contrast, the thicker sample B shown in Fig. 1 (left) has its third miniband localized entirely within the rectangular part of the AlN barrier, resulting in a small lateral displacement for the $2 \rightarrow 3$ transition. Furthermore, samples C and D yield considerably larger lateral displacements for transitions between the second and the third miniband d_{23}, than between

[a)]Electronic mail: daniel.hofstetter@unine.ch.

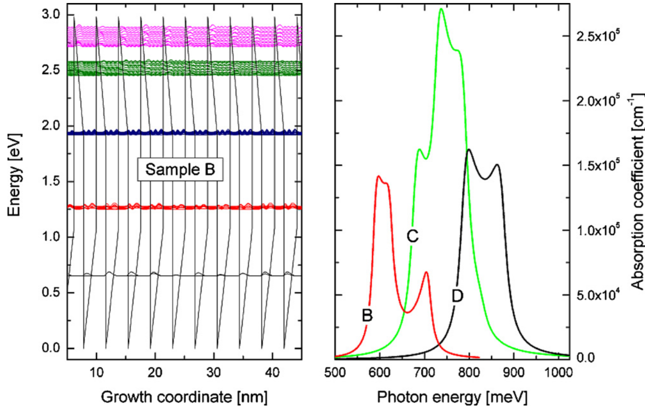

FIG. 1. (Color online) (Left) Schematic conduction band diagram of a III-nitride based photodetector showing the lowest five minibands. Data correspond to sample B, with 1.7 nm wide AlN barriers and 2.1 nm wide GaN QWs. (Right) Simulated absorption spectra for samples B, C, and D.

the first and the second miniband d_{12} (d_{12}=0.85 Å and d_{23} =12.3 Å for sample D).

Figure 2 shows a simulation of the miniband dispersion in the four different superlattice samples. In order to match the observed ISB transition energies, QW thicknesses of 2.6, 2.1, 1.7, and 1.4 nm had to be used for samples A, B, C, and D, respectively. The data were obtained from curves, as shown in Fig. 1 (left). Based on this simulation, we observe that the widths of the minibands increase dramatically with increasing quantum number: roughly 5–20 meV for the first, 15–65 meV for the second, between 20 and 230 meV for the third, and finally between 70 and 450 meV for the fourth miniband.[8] In addition, the highest miniband of sample D is smeared out into the continuum. As shown especially well in the simulated absorption spectrum for sample D in Fig. 1 (right), transitions between single miniband states at the center (k=0) and the edge (k=π/a) of the mini-Brillouin zone have higher absorption coefficients than those in between.[9] All simulations were performed for a temperature of 300 K; in addition, a peak broadening of 30 meV was taken into account. The absorption spectra were calculated using the dispersion data of Fig. 2 and assuming an electron concentration, which guarantees a finite occupation of the second miniband (the exact value of the Fermi energy has been adjusted to obtain spectra, which reasonably fit the experimental curves).

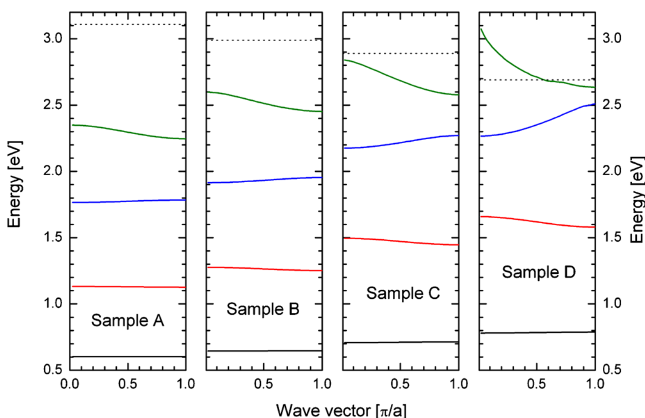

FIG. 2. (Color online) Superlattice dispersion curves for samples A, B, C, and D up to the fourth miniband. The dotted lines mark the onset of the continuum.

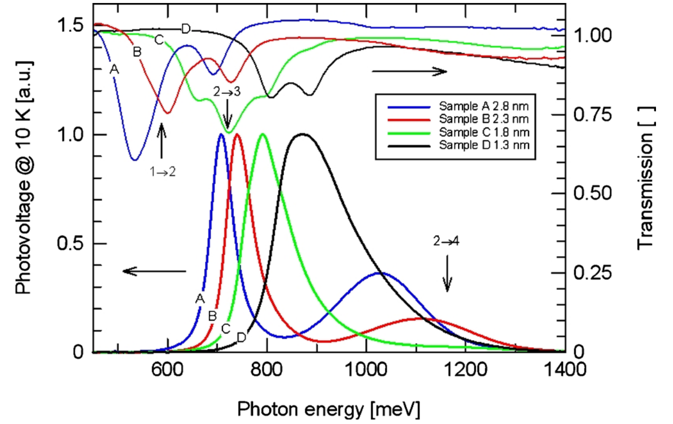

FIG. 3. (Color online) Transmission and photovoltage spectra of a series of AlN-GaN superlattice detectors. The normalized transmission curves are hanging from the upper x-axis while the photovoltage spectra stand on the lower x-axis. The vertical arrows indicate calculated transition energies for sample B, taken at the higher energy side.

In a next step, we performed different ISB spectroscopy experiments, most notably optical transmission and photovoltage. As a first example, we show in Fig. 3 room temperature ISB transmission spectra hanging from the top x-axis. As shown by vertical arrows for sample B, the observed energies of the transmission minima (absorption maxima) agree well to the ones obtained from our band structure calculations. The center wavelengths of the fundamental intersubband transitions between minibands $1\rightarrow2$ lie at 538, 600, 725, and 813 meV. At somewhat higher energy, transmission minima corresponding to the $2\rightarrow3$ transition at 688, 719, 788, and 888 meV are visible. For samples A and B, where the miniband widths are smaller than 50 meV, the minima of both transitions are well resolved and do not show any additional features. The absorbance ratios of their two corresponding transmission minima α_{12}/α_{23} are 1.7 (sample B) and 3.3 (sample A). Even when taking into account that the oscillator strength for the $2\rightarrow3$ transition is up to four times higher than for the $1\rightarrow2$ transition, this is a clear indication that both high sheet carrier density (as in samples A and B) and lateral carrier localization (as in samples C and D) result in a considerable population of the second miniband.

As explained previously, the $2\rightarrow3$ interminiband transition generates a pair of transmission minima separated by approximately the miniband width. Together with the two minima of the $1\rightarrow2$ interminiband transition, a sample can actually show up to four closely spaced absorption features. This is the case for sample C, whereas in sample D one of the $2\rightarrow3$ transition minima overlaps with the one of the $1\rightarrow2$ transition while the other one is *too small* to show up. The simulated absorption spectra in Fig. 1 (right) for samples B, C, and D correspond very well to the experimental transmission measurements. According to Tchernycheva *et al.*, such multiple transmission minima could also be due to monolayer fluctuations in the QWs.[10] Although this effect cannot be completely ruled out here, it would neither explain why only the *highest* energy absorption features produce a photovoltage nor result in more widely (closely) spaced transmission minima for thicker (thinner) QWs.

On the bottom x-axis of Fig. 3, 10 K photovoltage spectra of the four samples are presented. The peak energies—located at 706, 744, 800, and 875 meV for samples A, B, C, and D, respectively—are strongly shifted from the $1\rightarrow2$

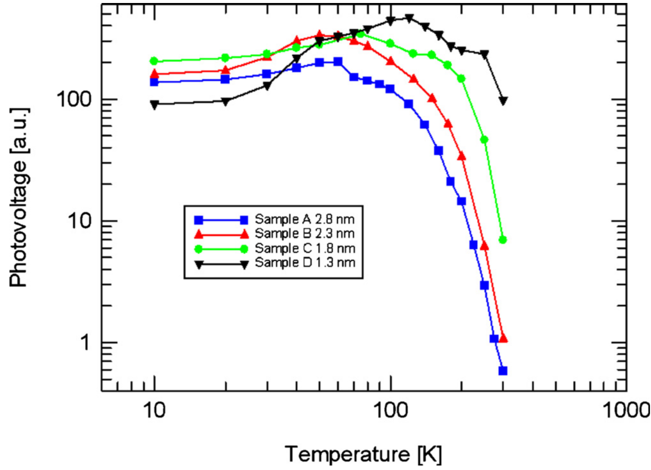

FIG. 4. (Color online) Photovoltages of the four samples as a function of temperature. The sample with the thinnest well, i.e., sample D, has the best performance.

transition energies obtained via optical transmission; however, they *much* better correspond to the simulated $2 \rightarrow 3$ transition energies. The remaining disagreement is due to inaccuracies of the model and an insufficient knowledge of the GaN/AlN material parameters. In any case, the only partial population of the second miniband favors transitions with a wave vector close to π/a, which have higher energies than those close to the mini-Brillouin zone center. Furthermore, these observations are justified by the small lateral electron displacement occurring in the $1 \rightarrow 2$ transition, due to which the optical rectification signal will be nearly zero. In contrast, between minibands 2 and 3, both dipole matrix element and lateral electron displacement can be much larger. Additionally, the relatively strong diagonality of this transition results in a prolonged electron lifetime. Therefore, a photovoltage measurement of a highly doped sample will essentially probe the $2 \rightarrow 3$ transition while the $1 \rightarrow 2$ transition shows up in transmission only. The photovoltage of samples A and B shows an additional, however, broad peak at 1050 (sample A) and 1130 meV (sample B). This is the transition between minibands 2 and 4, where miniband 4 starts to be very close to the continuum above the QWs. Although parity renders this transition relatively improbable, its considerable electron displacement makes it nevertheless visible for photovoltage. For the thinner samples, it can no longer be observed since miniband 4 gets pushed entirely into the continuum.

As outlined in our earlier paper on optical nonlinearities in GaN QW samples, photovoltage peaks at twice the transition energy occur if resonance between minibands 1 and 2 and minibands 2 and 3 is present.[5] These peaks are expected to *disappear* as soon as the three minibands move out of resonance. This has been verified in a logarithmic plot of the photovoltage spectra: The thinner samples C and D show the nonlinear peaks at twice the main transition energy, i.e., at 1750 and 1625 meV, whereas sample A shows no such peak at all (*not shown*).

Figure 4 displays the signal strengths of all four photodetectors as a function of temperature. Their responsivities are comparable at 10 K, increase up to about 50–120 K, and then decrease toward room temperature. Compared to the thickest QWs in sample A, sample D has a 200 times higher room temperature response. The slight increase in the response at low temperatures is attributed to the carrier density increase due to ionization of Si donors. Regarding the drop of the responsivity at high temperatures, two mechanisms contribute to this observation. First, electron-LO-phonon scattering decreases the lifetime of electrons in the third miniband for both larger QWs and higher sample temperatures.[11] Second, our band structure calculations have shown that the electron displacement of the $2 \rightarrow 3$ transition drops dramatically as soon as the third miniband is no longer localized in the triangular part of the AlN barrier. For samples with the third miniband close to the transition triangular/rectangular barrier, small temperature changes have therefore large effects on both electron displacement and observed signal strength.

Thanks to a combination of theoretical band structure calculations and different spectroscopic tools such as ISB transmission and photovoltage measurements, we were able to unambiguously identify up to four minibands occurring in 1.3–2.8 nm wide GaN-based QWs. In addition, we have shown that the operation of ISB photodetectors based on III-nitride superlattices relies on the ISB transition between the second and third minibands rather than between the first and second minibands. Although the second miniband is less populated with electrons, the $2 \rightarrow 3$ transition profits from a stronger dipole matrix element, a considerably larger lateral electron displacement, and a longer electron lifetime compared to the $1 \rightarrow 2$ transition.

This work was initiated by the Gebert-Ruef Foundation (GRS-044/06) and financially supported by armasuisse (AS-040/19). The AlN-on-sapphire templates used as substrates were provided by DOWA Electronics Materials Inc. High resolution x-ray measurements performed by Dr. Lutz Kirste (Fraunhofer IAF, Freiburg, Germany) are gratefully acknowledged.

[1] D. Hofstetter, S.-S. Schad, H. Wu, W. J. Schaff, and L. F. Eastman, Appl. Phys. Lett. **83**, 572 (2003).
[2] A. Vardi, N. Kheirodin, L. Nevou, H. Machhadani, L. Vivien, P. Crozat, M. Tchernycheva, R. Colombelli, F. H. Julien, F. Guillot, C. Bougerol, E. Monroy, S. Schacham, and G. Bahir, Appl. Phys. Lett. **93**, 193509 (2008).
[3] D. Hofstetter, J. Di Francesco, P. K. Kandaswamy, A. Das, S. Valdueza-Felip, and E. Monroy, IEEE Photonics Technol. Lett. **22**, 1087 (2010).
[4] E. Rosencher, Ph. Bois, B. Vinter, J. Nagle, and D. Kaplan, Appl. Phys. Lett. **56**, 1822 (1990).
[5] D. Hofstetter, E. Baumann, F. R. Giorgetta, F. Guillot, S. Leconte, and E. Monroy, Appl. Phys. Lett. **91**, 131115 (2007).
[6] D. Hofstetter, E. Baumann, F. R. Giorgetta, M. Graf, M. Maier, F. Guillot, E. Bellet-Amalric, and E. Monroy, Appl. Phys. Lett. **88**, 121112 (2006).
[7] P. K. Kandaswamy, F. Guillot, E. Bellet-Amalric, E. Monroy, L. Nevou, M. Tchernycheva, A. Michon, F. H. Julien, E. Baumann, F. R. Giorgetta, D. Hofstetter, T. Remmele, M. Albrecht, S. Bilner, and L. Si Dang, J. Appl. Phys. **104**, 093501 (2008).
[8] B. K. Ridley, J. Appl. Phys. **94**, 3972 (2003).
[9] M. Helm, W. Hilber, T. Fromherz, F. M. Peeters, K. Alavi, and R. N. Pathak, Phys. Rev. B **48**, 1601 (1993).
[10] M. Tchernycheva, L. Nevou, L. Doyennette, F. H. Julien, E. Warde, F. Guillot, E. Monroy, E. Bellet-Amalric, T. Remmele, and M. Albrecht, Phys. Rev. B **73**, 125347 (2006).
[11] H. Froehlich, H. Pelzer, and S. Zienau, Philos. Mag. **41**, 221 (1950).